JOURNAL OF GEOPHYSICAL RESEARCH, VOL. 95, NO. C7, PAGES 11,655–11,672, JULY 15, 1990

Southern Ocean Winter Mixed Layer

ARNOLD L. GORDON AND BRUCE A. HUBER

Lamont-Doherty Geological Observatory, Columbia University, Palisades, New York

Austral winter 1986 observations from the *Polarstern* along the Greenwich meridian from the ice edge to the Antarctic margin show the mixed layer beneath the winter sea ice cover to be significantly depressed in oxygen saturation. Incorporation of Weddell Deep Water (WDW) into the winter mixed layer, responsible for this undersaturation, also introduces heat and salinity into the surface layer which strongly influences the mixed layer, sea-air exchanges and sea ice formation processes. The total WDW transfer into the mixed layer averages 45 myr^{-1}, implying a residence time for the surface water of 2.5 years. The associated winter heat flux is 41 W m^{-2}, which limits ice thickness to about 0.55 m, agreeing quite well with observations. The air temperatures during the cruise are just sufficient to remove the WDW heat input in the presence of observed ice thickness and concentration. This suggests that the sea ice cover and WDW heat input into the mixed layer are in approximate balance by midwinter. The annual heat flux from WDW to the surface layer, and hence into the atmosphere, is estimated as 16 W m^{-2}. Extrapolation of the Greenwich meridian WDW entrainment value to the full circumpolar 60°–70°S belt yields total upwelling of 24 × 10^{6} m^{3} s^{-1}. Similar extrapolation of the heat flux value gives a circumpolar total of 2.8 × 10^{14} W. As a consequence of circulation/topography interaction, the Maud Rise water column stands out as an anomaly relative to the surrounding region, with a significantly more saline and dense mixed layer. Below the mixed layer the water column over the crest of the rise is identical to that over the flanks if the latter water column is upwelled by 400 m. This uplifting is believed to be a response of the upstream flow encountering the rise. Increased upstream flow would be expected to increase Maud Rise upwelling and the dependent salinity (density) of the mixed layer. Slight increases in the mixed layer density could trigger a convective mode and generation of a polynya. It is hypothesized that spin-up of the Weddell Gyre's barotropic circulation induced by an increase of the regional wind stress curl would enhance the probability of polynya development over Maud Rise.

1. INTRODUCTION

Measurements made during austral spring 1981 from the *Mikhail Somov* of the ocean beneath the sea ice cover from 56° to 62.5°S near the Greenwich meridian provide evidence for significant amounts of deepwater incorporation into the winter mixed layer [*Gordon et al*, 1984; *Gordon and Huber*, 1984]. Associated vertical flux of heat, salt, and gases have important effects on sea-air exchanges and sea ice characteristics and may also be of some importance to the larger climate [*Gordon*, 1988]. From July 7 to September 9, 1986, cruise Ant V/2 (a component of the Winter Weddell Sea Project 1986 [*Schnack-Schiel*, 1987]) of the Federal Republic of Germany (FRG) research icebreaker *Polarstern* carried out an observational study of the winter ocean, atmosphere, and sea ice characteristics along the Greenwich meridian from the ice edge to the continental margins of Antarctica (Figure 1).

The Weddell Gyre is a large cyclonic circulation cell extending from the Antarctic Peninsula to approximately 30°E, with the baroclinic circulation trough or gyre "hub" intersecting the Greenwich meridian between 60° and 62°S [*Deacon*, 1979; *Gordon and Huber*, 1984; *Whitworth and Nowlin*, 1987; *Comiso and Gordon*, 1987; *Bagriantsev et al.*, 1989]. The northern boundary of the gyre at the Greenwich meridian, marking the sharp transition to the circumpolar belt, occurs near 56°S, coinciding with the winter maximum extent of the sea ice cover. The southern and western boundaries of the gyre are formed by the continental margin of Antarctica. The northern limb of the Weddell Gyre is dominated by easterly flow, advecting a very cold water column away from the gyre's western boundary current. South of the gyre trough the flow is toward the west, recirculating cold interior waters and in closer proximity to Antarctica, advecting westward the relatively warm Circumpolar Deep Water (CDW) which sweeps into the gyre's eastern margins. The details of the eastern boundary are not well resolved; possibly, it is at this boundary that the gyre interacts most freely with the circumpolar water masses at all depths.

This study focuses on the upper ocean. We (1) quantify significant deepwater incorporation into the sea-ice-covered winter mixed layer, with accompanied vertical fluxes of heat and salinity, across the full latitudinal extent of the Weddell Gyre; (2) discuss the overall harmony of ice thickness with the underlying ocean fluxes; (3) discuss the anomalous stratification over Maud Rise; and (4) present thoughts regarding the impact of these results on the full circumpolar belt and on polynya generation. It is noted that we often use the word "entrainment," by which we mean the incorporation of Weddell Deep Water (WDW) characteristics into the mixed layer. The companion paper by *Martinson* [this issue] models the responsible processes.

2. LARGE-SCALE FEATURES

To provide background, the large-scale thermohaline field as viewed with the Ant V/2 data set is briefly presented.

2.1. *Temperature and Salinity Sections*

The full depth temperature, salinity, and sigma-zero sections reveal the nearly homogeneous nature of the thermohaline structure characteristic of the zone poleward of the Antarctic Circumpolar Current (Figures 2*a*–2*c*; the complete set of sections are included in the Ant V/2 data report

Paper number 90JC00444.
0148-0227/90/90JC-00444$05.00

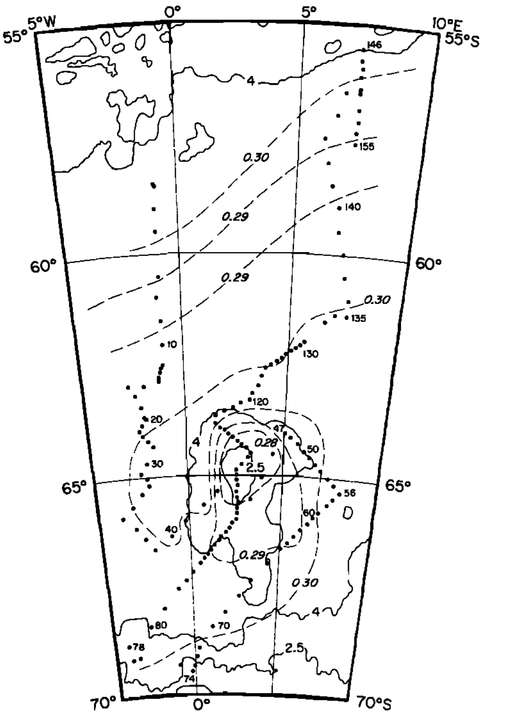

Fig. 1. CTD stations obtained during *Polarstern* cruise Ant V/2. The 2.5- and 4-km isobath indicates the position of Maud Rise centered at 65°S and 2.5°E, the continental margin near 70°S, and the polar flank of the mid-ocean ridge near 55°–57°S. The light dashed lines show the sea surface dynamic height anomaly in dynamic meters, relative to the 1000-dbar surface.

[*Huber et al.*, 1989]). The temperature maximum (t-max) in the 200- to 500-m range marks the "top" of the WDW [*Bagriantsev et al.*, 1989] drawn into the gyre from the lower stratum of the CDW [*Gordon and Huber*, 1984; *Whitworth and Nowlin*, 1987]. The poleward edge of CDW, marking the northern boundary of the Weddell Gyre, is observed at station 145. Within the Weddell Gyre the t-max is not a uniform sheet; rather, it is composed of patches that may reflect circulation patterns. Slightly deeper than the t-max is a salinity maximum (s-max). Below the WDW s-max the thermohaline stratification is minor, amounting to a total range of only 1°C, 0.03 practical salinity units (psu), and 0.05 sigma-zero. The slightly colder and less saline bottom water in the northern end of the sections is the more concentrated Antarctic Bottom Water (AABW) flowing from the western boundary region. Along the southern boundary, the increased slope of the isopleths indicates a baroclinic westward flowing slope current, the prime source of heat and salt for the Weddell Sea and western margins of the gyre. A further increase in isopleth slopes is observed in the vicinity of Maud Rise. Maud Rise dominates the bottom topography of the Weddell Gyre near the Greenwich meridian, reaching a minimum depth of 1631 m, with a meridional expression of roughly 400 km (about the same in the zonal direction) at the 3000-m level.

A revealing way to exhibit the thermal field across Maud Rise is to use sigma-zero as the vertical coordinate (Figure 3). The varied density of the surface water, along with the t-max stratum, dominates the structure. The deep and bottom water are portrayed as a thin band, with Maud Rise hardly more than a bump. The relatively dense surface water over Maud Rise sharply decreases the density range over the crest of the rise. It is noted that the surface water over the rise has roughly the same sigma-zero as the t-max water over the rise flanks, allowing isopycnal mixing between the t-max and the Maud Rise mixed layer, as discussed in section 6 of this study.

The focus of this paper is on the upper ocean, so attention is drawn to the sections for the upper 1000 m (Figure 4), above the sill depth of Maud Rise, but not above its influence on the stratification. There are distinct meridional variations in the nature of the temperature and salinity maxima of the WDW, as well as variations of the mixed layer depth and thermohaline characteristics. The broad region with WDW potential temperature maximum of near 0.4°C and 34.68 salinity, from 57°S to 62.5°S, defines the cold regime of the Weddell Gyre [*Gordon and Huber*, 1984]. It is composed of the eastward flowing northern limb and trough of the Weddell Gyre plus the northern part of the return flow. Within this regime the isotherms and isohalines are rather flat, with a mixed layer thickness of approximately 125 m.

Near 62.5°S there is an abrupt change in deepwater and mixed layer characteristics. The warmer and saltier WDW south of 62.5°S is due to incorporation of CDW drawn into the gyre from the east [*Gordon and Huber*, 1984 ;*Whitworth and Nowlin*, 1987]. The warmest WDW along the Greenwich meridian occurs over the flanks of Maud Rise. A map view of the t-max using the full Ant V/2 data set (Figure 5, left) shows that WDW of temperature greater than 1°C does not form a complete halo, though all stations over the flanks have deepwater temperatures well above that found over the crest of Maud Rise. *Bagriantsev et al.* [1989] show that in 1984 austral summer a large pool of warmer deep water occurred just to the west of Maud Rise, and they speculate that it is a quasi-stationary feature.

South of Maud Rise the mixed layer is 0.1°C warmer and over 0.1 psu higher in salinity than it is within the cold regime to the north. Over Maud Rise the mixed layer salinity exceeds 34.5 (Figure 5, right), inducing a σ_0 difference between t-max and mixed layer of slightly less than 0.04 (also see Figure 3). This induces a baroclinic cyclonic circulation over the rise with a rather sharp front at the edges of the Maud Rise water column (Figure 1).

2.2. *Property/Property Relationships*

2.2.1. *Potential temperature–salinity, θ/S relation.* The mixed layer θ/S characteristics (Figure 6*a*), are exhibited as a scatter of points slightly offset from the freezing line, spanning the salinity interval from 34.15 to 34.52, representing 80% of the full water column density (σ_0) range, though only 2% of the water column. Many of the individual stations exhibit a small salinity increase (about 0.005) toward the mixed layer base, with an associated slightly warmer temperature. In the context of the WDW entrainment argument presented later, this may be taken as a sign of WDW characteristics invading the lower segment of the mixed layer, indicating that blending of water types within the mixed layer is not immediate. Maud Rise station 103 represents the high-salinity limits of the mixed layer and pycnocline. The CDW represented by station 146 defines the circumpolar source characteristics for the deep waters of the Weddell Gyre [*Gordon and Huber*, 1984; *Whitworth and Nowlin*, 1987].

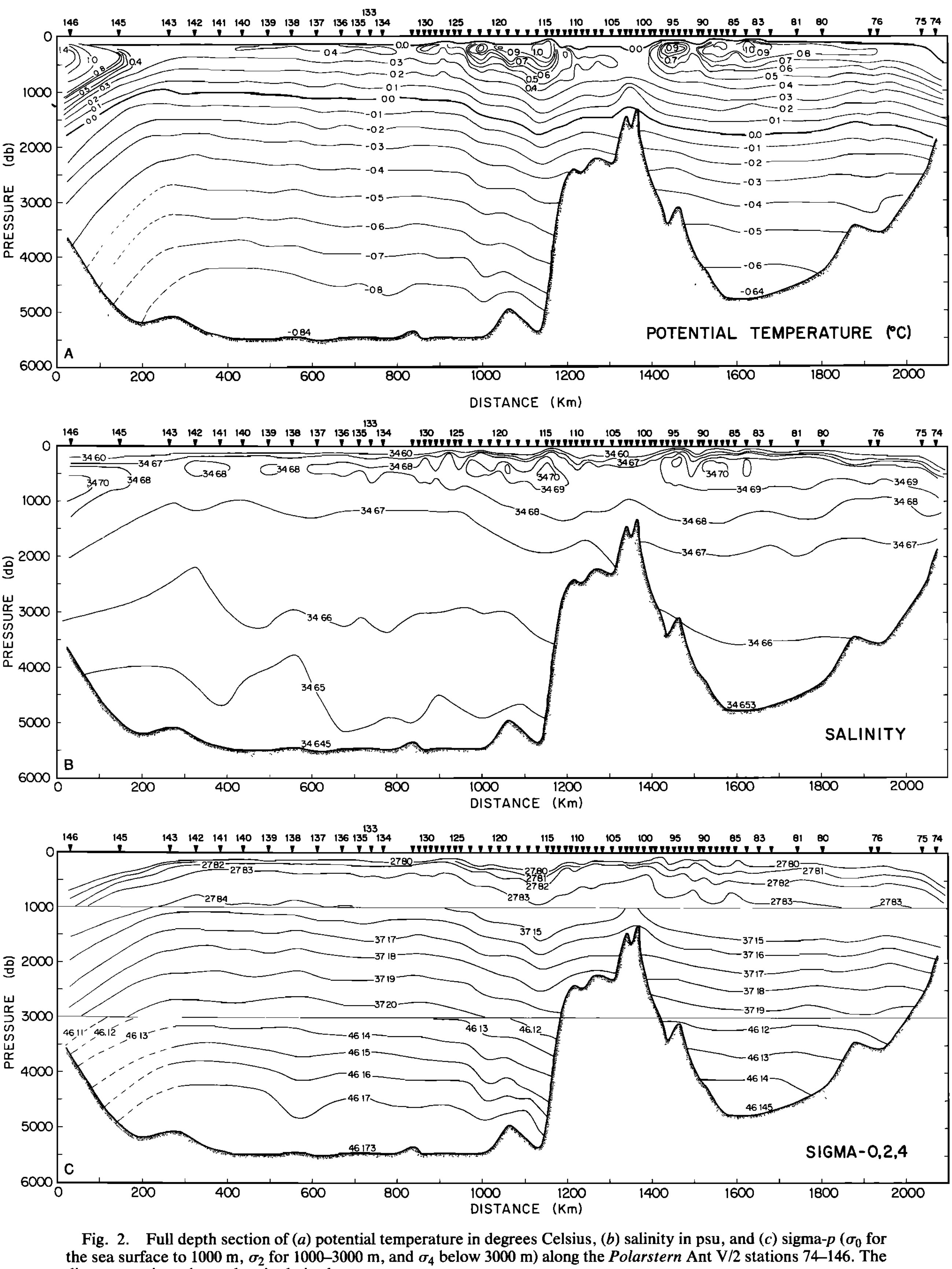

Fig. 2. Full depth section of (*a*) potential temperature in degrees Celsius, (*b*) salinity in psu, and (*c*) sigma-*p* (σ_0 for the sea surface to 1000 m, σ_2 for 1000–3000 m, and σ_4 below 3000 m) along the *Polarstern* Ant V/2 stations 74–146. The distance projected on a longitude is shown.

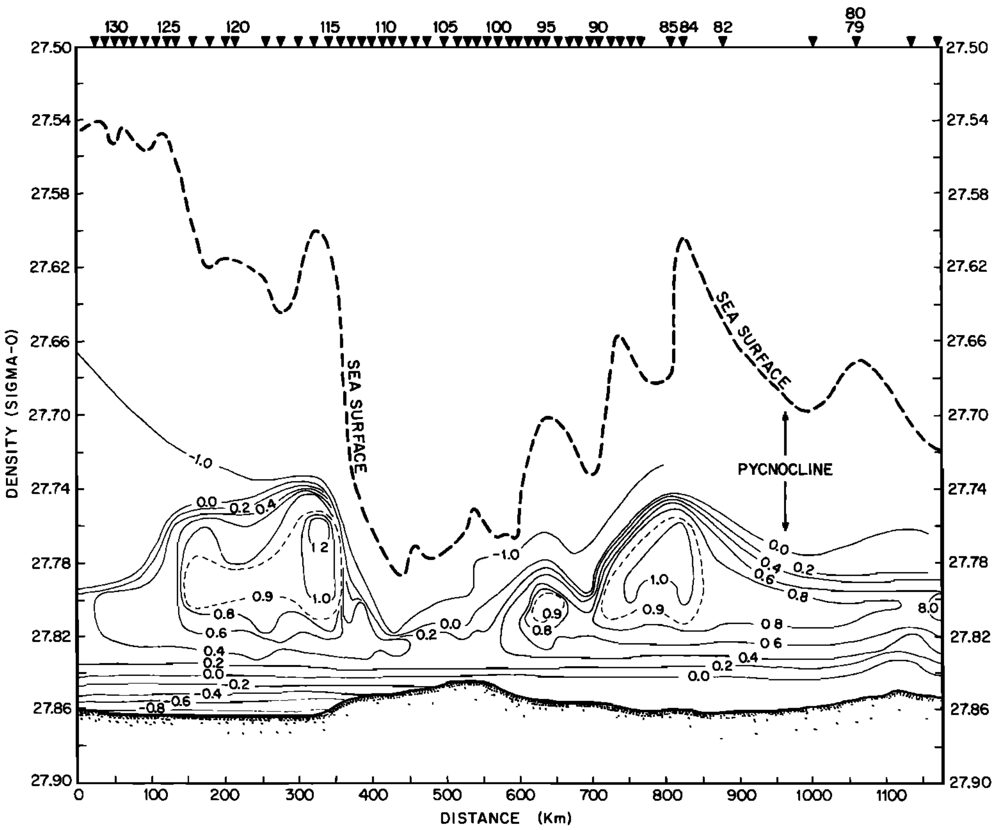

Fig. 3. Potential temperature for stations 77–132, crossing Maud Rise, with sigma-zero (σ_0) as the vertical coordinate.

The mixed layer has contact via a thin, weak pycnocline with the WDW-AABW θ/S sequence in the range of 0.3°–1.35°C and salinity 34.67–34.72. There are some nonlinear structures in the WDW-AABW θ/S sequence below the salinity maximum and within the bottom layer. These features are beyond the scope of this paper and will be included in a more complete discussion of the deepwater and bottom water masses of the Weddell Gyre.

2.2.2. *Potential temperature–oxygen, θ/O_2 relation.* The WDW-AABW θ/O_2 sequence (Figure 6*b*) reveals a nonlinear structure near 0.5°C. At warmer temperatures the θ/O_2 follows that of the CDW north of the Weddell Gyre [*Gordon and Huber*, 1984]. However, between 0.25° and 0.5°C a distinct oxygen minimum occurs. This feature is found primarily within the Weddell cold regime (where the WDW *t*-max is 0.5°C or less [*Gordon and Huber*, 1984]) and is associated with a nutrient maximum. This stratum is believed to be locally generated through oxygen utilization (see *Weiss et al.* [1979] and *Whitworth and Nowlin* [1987], who referred to it as "central intermediate water"). At colder temperatures, below any direct isopycnal connection to the open ocean winter mixed layer, there is a linear trend leading to AABW. Presumably within this segment of the WDW-AABW sequence, "communication" with the surface layer occurs within the continental margin regime.

Extension of the θ/S and θ/O_2 WDW-AABW sequence to the freezing point indicates the dominant cold water input to the bottom layer has an oxygen concentration of 6.8 mL/L and a salinity of 34.62. The same salinity and approximately the same oxygen was determined for the cold surface water input to bottom water formation in the Bransfield Strait [*Gordon and Nowlin*, 1978]. The cold surface end-member for AABW formation may be quite uniform around the periphery of the Weddell Gyre.

The mixed layer θ/O_2 scatter covers a wide range of oxygen values, approximately from 6.4 to 8.0 mL/L, representing a saturation range from 75% to 97%. This is presumed to be a product of incorporation of oxygen poor WDW into the winter mixed layer, the implications of which are explored in greater detail below. The water with oxygen near 8 mL/L and temperatures well above the freezing mark is the surface water along the northern boundary of the Weddell Gyre.

2.3. *Mixed Layer Detail*

The mixed layer observed during Ant V/2 forms a nearly homogeneous layer with an average thickness of 111 m (with a standard deviation of 33 m; Figure 7*a*). South of 62.5°S it is slightly shallower than the average, though over Maud Rise and along the continental margin it deepens. Within the cold regime the mixed layer is approximately 125 m thick. The pycnocline is generally weak, with a marked further weakening from Maud Rise to the continental margin (Figure 7*b*). Temperature, salinity, and oxygen profiles for the upper 250 m also demonstrate the regional differences (Figure 7*c*) in thickness and pycnocline intensity.

Mixed layer temperature and salinity increase abruptly south of 62.5°S, while oxygen saturation decreases (Figures 8*a*–8*c*). This latitude marks the separation of the Weddell cold and warm regimes. For example, in the latitude range of 65°–70°S the mixed layer temperature is 0.10°C above the

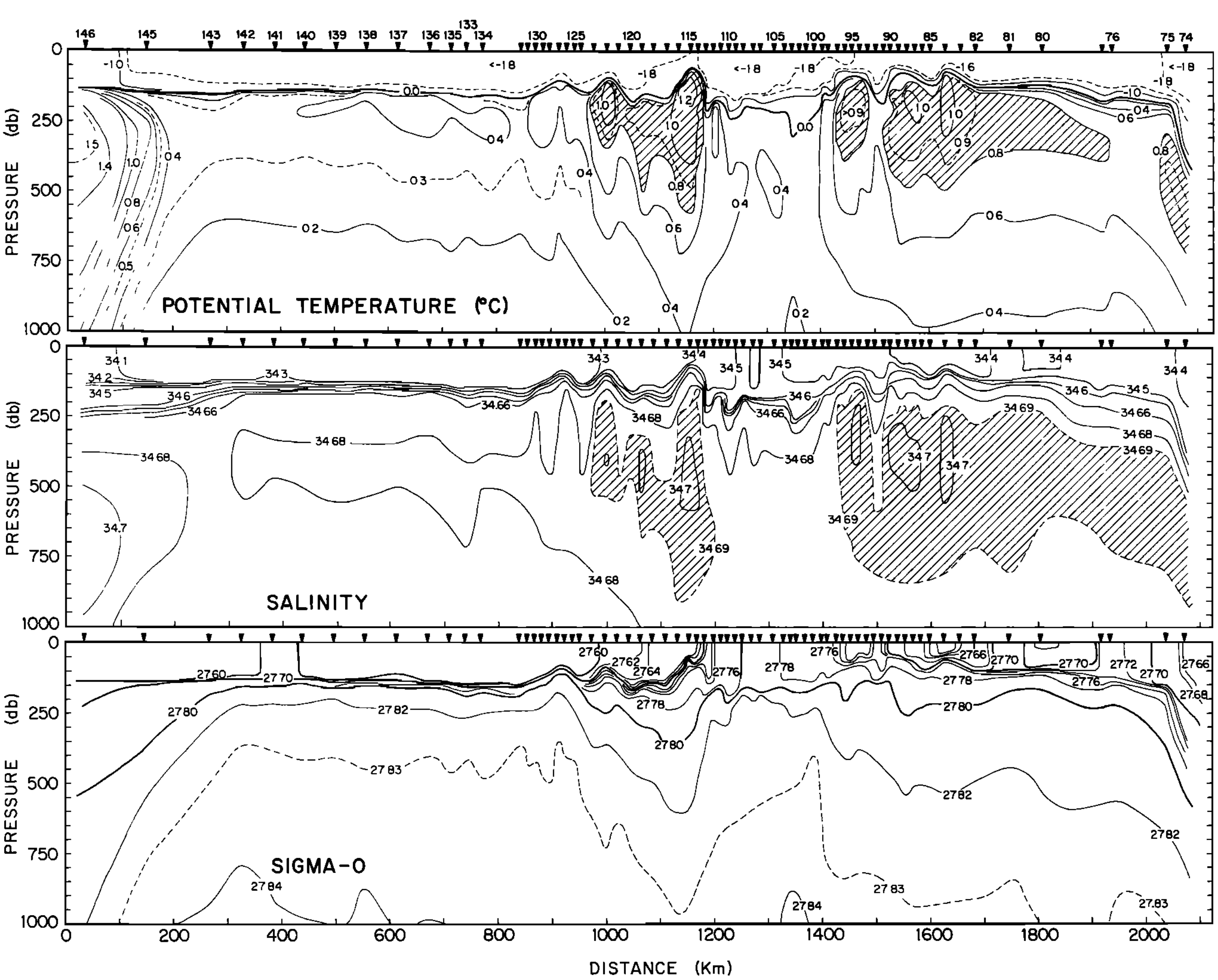

Fig. 4. Potential temperature, salinity, and sigma-zero for the upper 1000 m for the *Polarstern* Ant V/2 stations 74–146.

freezing point with an oxygen saturation of about 80%. North of 62.5°S the mixed layer averages only 0.025°C above freezing with an oxygen saturation of over 90%. The Maud Rise water column with a salinity of 34.5 is about 0.05°C above freezing with an oxygen saturation of 83–85%.

The salinity anomaly of the Maud Rise mixed layer is evident in θ/S space (Figure 9*a*) as a cluster of points with salinity values near 34.5. The S/O_2 saturation (Figure 9*b*) reveals a linear trend from the Weddell cold regime (about 34.2 psu and 94% oxygen saturation) to a point near 34.45 psu and 75% oxygen saturation. The Maud Rise water column deviates from this trend. The Maud Rise anomaly may represent a water column somewhat isolated during the entire year, allowing a general buildup of mixed layer salinity (which may be derived from enhanced upwelling over the rise; see section 6). Elevated salinity of the winter remnant temperature minimum (*t*-min) layer over Maud Rise relative to the regional value is observed in the Ajax summer data set [*Scripps Institution of Oceanography* (*SIO*), 1985].

In summary, the mixed layer property relationships reveal a positive correlation of oxygen undersaturation with both salinity and temperature. This is expected if WDW characteristics infiltrate the mixed layer, which we believe is occurring. Temperature and salinity are modified by exchanges with the atmosphere and ice, whereas the oxygen concentration may not be. This is the subject of the following section.

3. Deepwater Entrainment and Associated Heat Flux

3.1. *Entrainment Calculations*

Elevated mixed layer temperatures relative to the freezing point, accompanied by depressed oxygen concentrations and relatively high salinities, are indicative of significant incorporation of WDW properties into the winter mixed layer [*Weiss et al.*, 1979; *Gordon and Huber*, 1984]. Mixed layer entrainment of WDW can be driven by turbulence produced by relative ice motion and by convection stemming from ice formation [*Martinson*, this issue]. Entrainment processes sharpen and deepen the pycnocline as the mixed layer incorporates WDW into its volume during the winter period. This is countered on the annual scale by Ekman upwelling. Vertical diffusion tends to diminish the gradient of the pycnocline throughout the year. The seasonal evolution of the mixed layer and transitional pycnocline depend on the balance of these processes, which are sensitive to sea

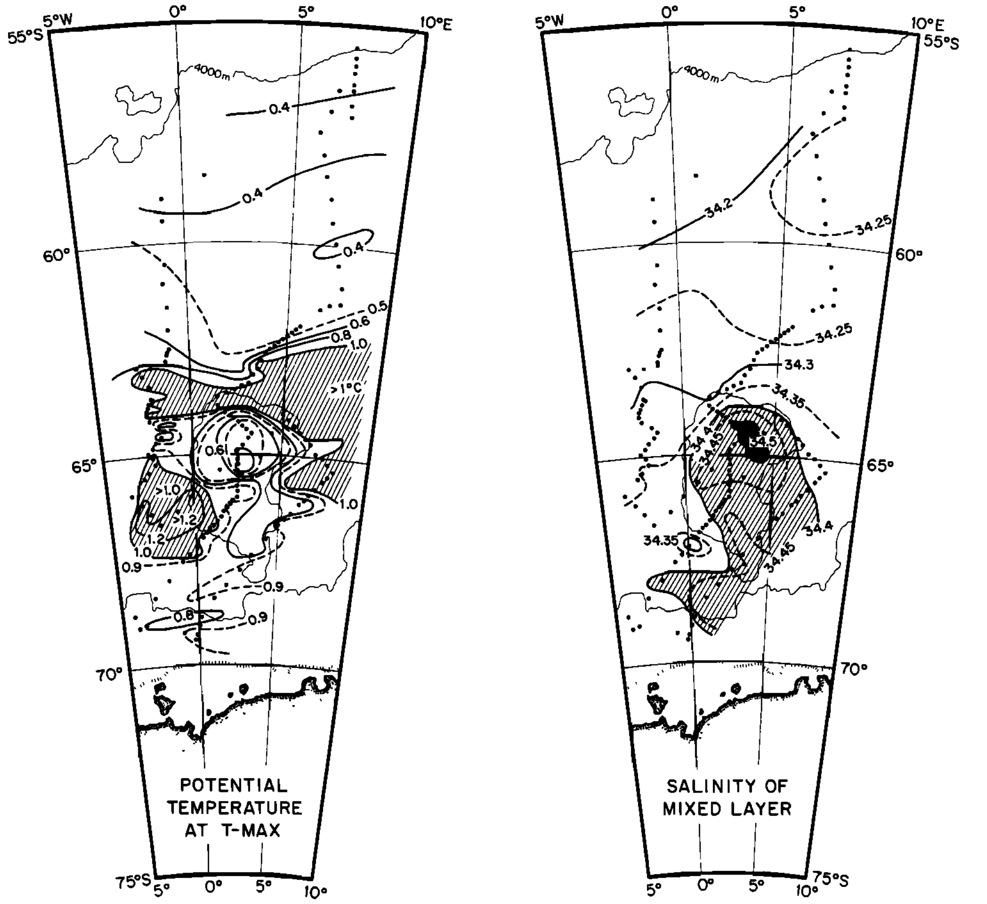

Fig. 5. (Left) Potential temperature maximum map and (right) mixed layer salinity map. The mixed layer parameters used in the salinity map, as well as in other representations of mixed layer properties referred to in this paper, are obtained by averaging all rosette bottle derived sample levels in the more or less well mixed central stratum of the mixed layer from 25 to 60 m depth.

ice dynamics and thermodynamics which in turn respond to atmospheric forcing.

Formation of sea ice does not require the entire mixed layer to be at the freezing point (t_f). For sufficiently low air temperatures, ice will form on a thin sublayer whose temperature is t_f, with the bulk of the mixed layer at a slightly higher temperature [*Røed*, 1984; *Houssais*, 1988]. The difference between bulk mixed layer temperature and t_f (given by δt) supports a heat flux from the mixed layer through the ice to the atmosphere. For the observed average δt = 0.08°C, the flux is estimated to be

$$F_{aw} = K_w\ (\delta t) = 22 \text{ W m}^{-2}$$

where k_w = 270 W m^{-2} s^{-1}°C^{-1} is the bulk ocean-ice heat transfer coefficient [*Røed*, 1984; *Houssais*, 1988]. Heat flux of this magnitude would reduce δt to zero in 2–3 weeks. Thus the elevated temperatures of the mixed layer cannot be a remnant of the previous summer and must be supported by active entrainment.

The WDW heat input to the mixed layer is lost to the atmosphere through the sea ice and its leads, and therefore it is not possible to determine the amount of entrainment directly from the temperature data. Is it not possible to do so from the salinity of the mixed layer either, since sea ice freezing and melting alters the mixed layer salinity. However, it is possible to estimate the total entrainment during the ice-covered period using the oxygen concentration as a proxy, with two assumptions:

1. The oxygen concentration is essentially conservative; it is not influenced by the biological processes under the sea ice. This assumption is well supported by the dissolved anthropogenic chlorofluorocarbons (CFC) F-11 and F-12 obtained during Ant V/2 [*Weiss*, 1987], which are essentially biologically inert. The mixed layer has a CFC F-11 saturation ranging from 46 to 85%. The deep water is essentially devoid of CFC, so a 50 : 50 mix of deep water with initially saturated surface water would yield a 50% CFC saturated mixed layer. The corresponding oxygen saturation would be 80%, since the WDW oxygen saturation is approximately 60%. Comparison of the mixed layer CFC concentration (provided by R. Weiss (personal communication, 1987) based on preliminary CFC data) versus that of the oxygen yields a linear relation with a correlation coefficient of 0.98. Therefore the oxygen and CFC would yield virtually the same entrainment levels, and the effects of biology can be neglected.

2. There is no significant oxygen flux across the snow-covered sea ice, which had a mean concentration of 95% during Ant V/2 [*Wadhams et al.*, 1987]. Sea ice cover inhibits gas exchange with the atmosphere [*Schlosser et al.*, 1987]. Use of CFC does not help here, since its exchange characteristics are expected to be similar to those of oxygen. Oxygen undersaturation in winter mixed layers even without

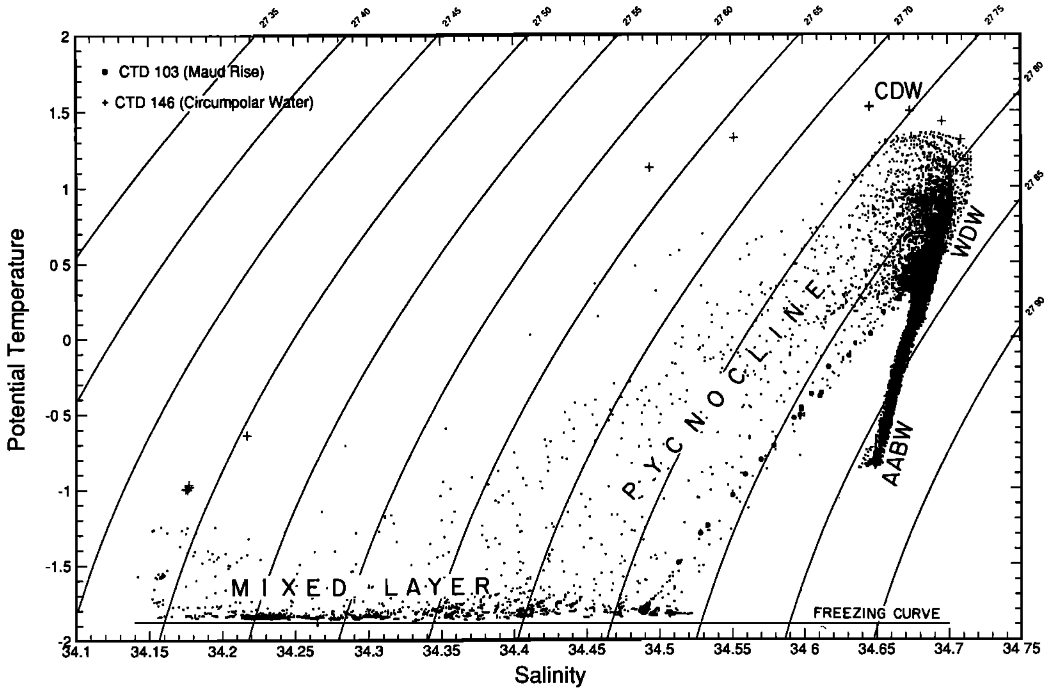

Fig. 6*a*. Potential temperature and salinity relationship for all of the Ant V/2 CTD stations shown in Figure 1. Each θ/S point represents a 10-dbar interval. Station 103 represents the water column over Maud Rise. Station 146 falls within the circumpolar water regime north of the Weddell Gyre.

a sea ice cap has been reported [*Reid*, 1983; *Clarke et al.*, 1990]. Recognizing that there might be some exchange, particularly through the leads (observed to amount to about 5% during Ant V/2), it is noted that the mixed layer is undersaturated; hence any exchange with the atmosphere would transfer oxygen into the ocean, and the calculations presented below would therefore represent a lower bound of deepwater entrainment into the mixed layer.

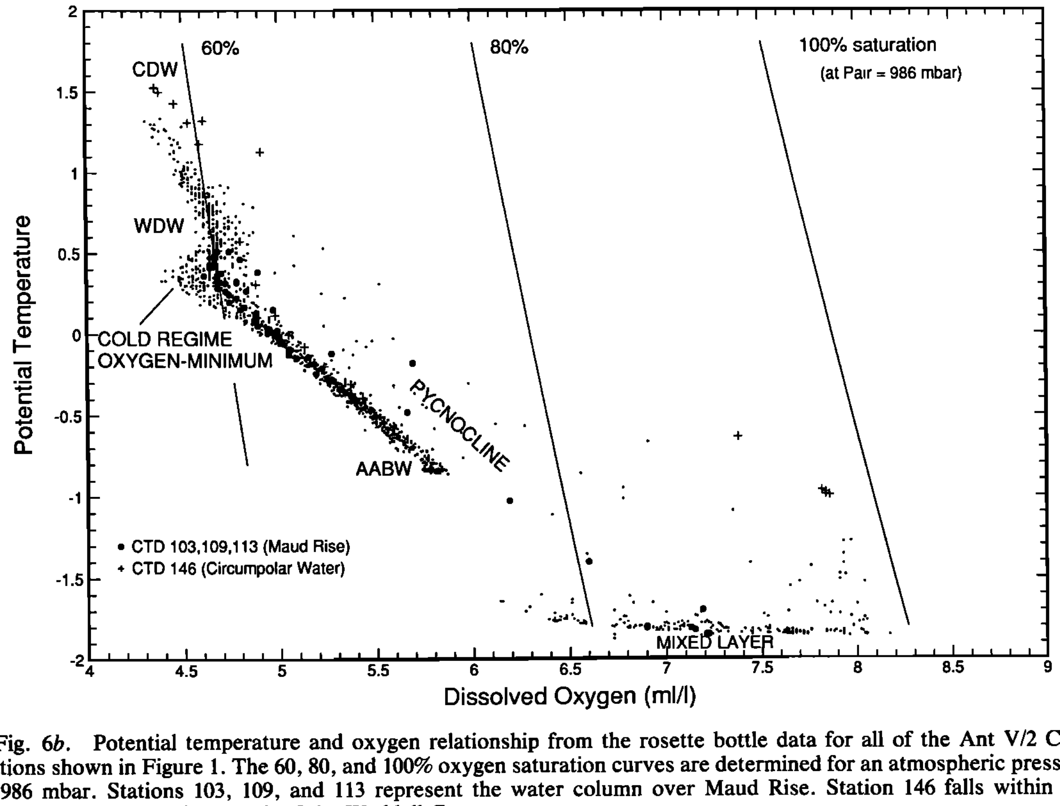

Fig. 6*b*. Potential temperature and oxygen relationship from the rosette bottle data for all of the Ant V/2 CTD stations shown in Figure 1. The 60, 80, and 100% oxygen saturation curves are determined for an atmospheric pressure of 986 mbar. Stations 103, 109, and 113 represent the water column over Maud Rise. Station 146 falls within the circumpolar water regime north of the Weddell Gyre.

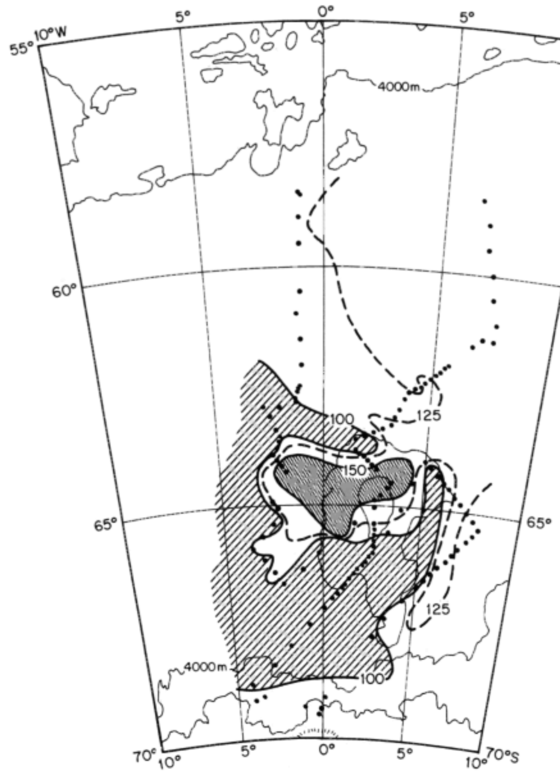

Fig. 7*a*. Mixed layer thickness map in meters.

With these assumptions the total amount of deep water incorporated into the mixed layer from the start of the entrainment (winter) period to the time of the observations can be determined. First, the initial mixed layer oxygen concentration must be determined. While the summer mixed layer oxygen is usually at or slightly above full saturation, rapid cooling of the surface layer prior to the onset of ice formation may lower the saturation level faster than sea-air gas exchange can restore equilibrium. For a nominal wind speed of 12 m s^{-1} and a water temperature of -1°C the exchange velocity of oxygen can be computed using the formulation of *Liss and Merlivat* [1986] as 15.5 cm h^{-1} which yields a time constant of 27 days for a 100-m mixed layer. (We note too from this that exchange of oxygen through an ice cover with 5% leads would have an effective time constant of >400 days. Mixed layer deepening due to rapid cooling following cold air outbreaks has been observed to occur on time scales of 1–2 days [*Shay and Gregg*, 1986]. Therefore less than 100% oxygen saturation in a fall season mixed layer, before ice formation, is feasible and perhaps expected. Undersaturation in the ice-free ocean under buoyancy removal conditions has been observed in the winter Greenland Sea, seaward of the ice edge [*Reid*, 1983].

An additional effect is as follows: as deepening of the fall season mixed layer proceeds, the undersaturated water from the winter remnant *t*-min is mixed with near-surface water. The average oxygen concentration, and therefore saturation level, of such a mixed layer can be estimated from summer data if one assumes that the summer oxygen profile is simply mixed to the *t*-min depth, rapidly enough so exchange with the atmosphere is negligible. Using Ajax stations 81–94 [*SIO*, 1985] (section along the Greenwich meridian), the average oxygen concentration of the resulting mixed layers is 7.97 ± 0.13 mL/L.

The Ant V/2 data can be used to estimate the mixed layer oxygen saturation at the onset of the winter sea ice cover by relating observed oxygen undersaturation to the number of days under ice at each conductivity, temperature, and depth (CTD) station site (Figure 10). The 100% oxygen saturation value is determined for an air pressure of 986 mbar, which is the average summer value (before the mixed layer is decoupled from free gas exchange with the atmosphere), given for the region by *Van Loon* [1972]. The days under sea ice are

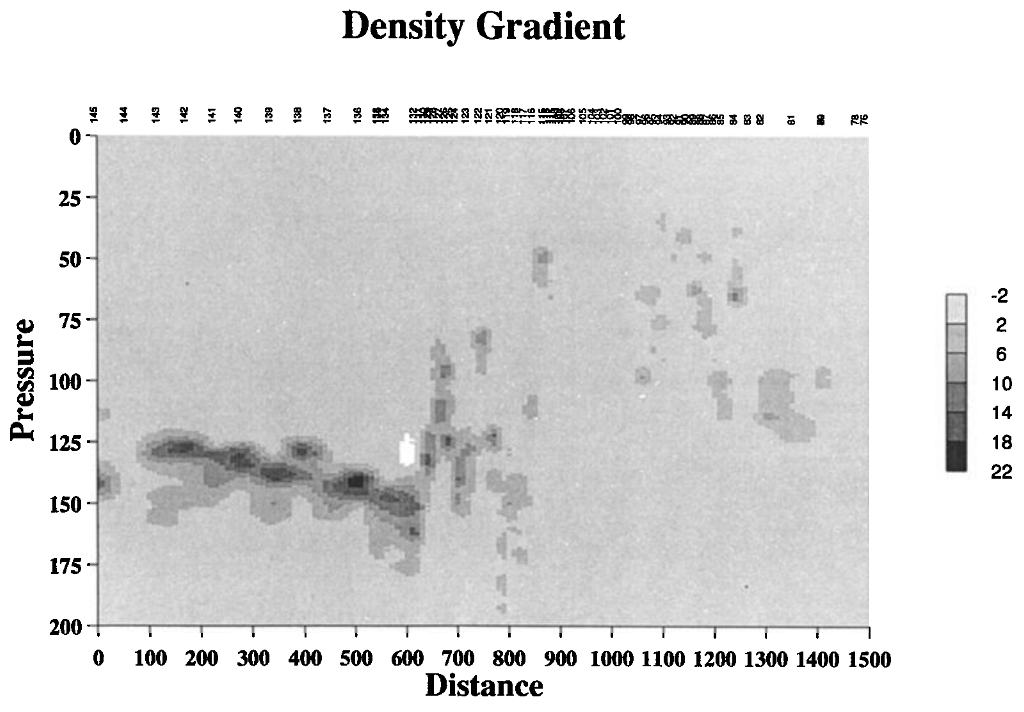

Fig. 7*b*. Sigma-zero gradient within upper 200 m, expressed in sigma-zero change per meter.

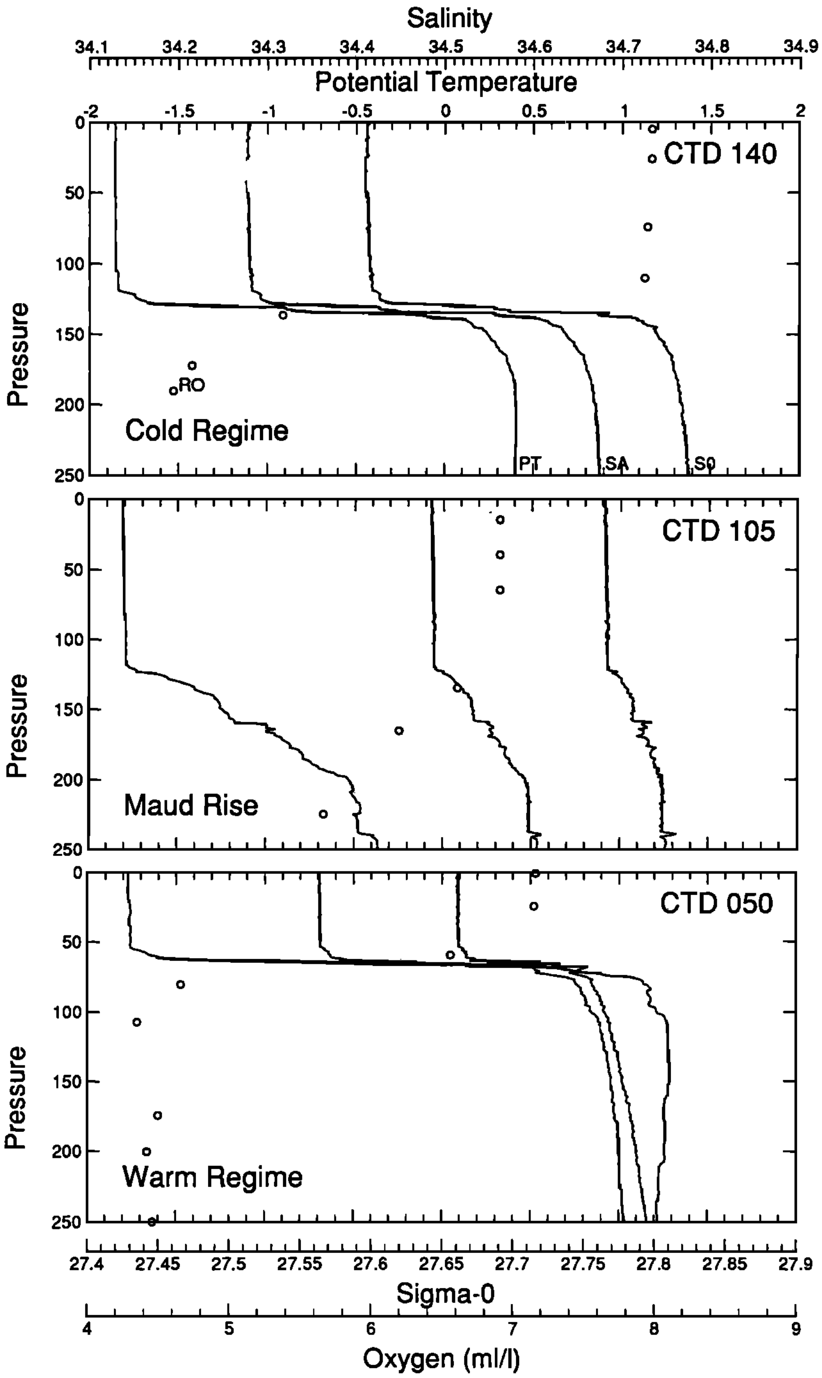

Fig. 7*c*. Typical mixed layer structures in temperature, salinity, and density stratification in each of the major oceanographic regimes encountered during *Polarstern* Ant V/2.

determined by differencing the day of the CTD observation from the time of the first ice cover, as defined by the Navy-National Oceanic and Atmospheric Administration (NOAA) ice charts. Oxygen saturation decreases linearly (correlation coefficient of 0.81) with increasing time below the sea ice. The relationship indicates that the oxygen saturation near the time of onset of the winter sea ice cover (day 0) is 96.1% or 7.94 mL/L at an air pressure of 986 mbar, agreeing with the value computed from Ajax data [*SIO*, 1985]. We will therefore use our estimate of 7.94 mL/L (96% oxygen saturation) as an initial condition in the following analysis.

The initial mixed layer is taken at −1.8°C (slightly above the freezing point since, as mentioned above, a freezing point mixed layer is not required or expected at the onset of sea ice formation; use of the freezing point does not significantly alter the results), with 7.94 mL/L oxygen concentration; the WDW mean oxygen concentration of 4.65 mL/L is used with the observed *t*-max at each station. An estimate is then derived for the mixed layer temperature at the time of observation if it was capped by a perfect insulating lid. The heat (relative to freezing) that has been incorporated into the mixed layer since the beginning of the entrainment process is given by Q_t (in joules per square meter; Figure 11). This

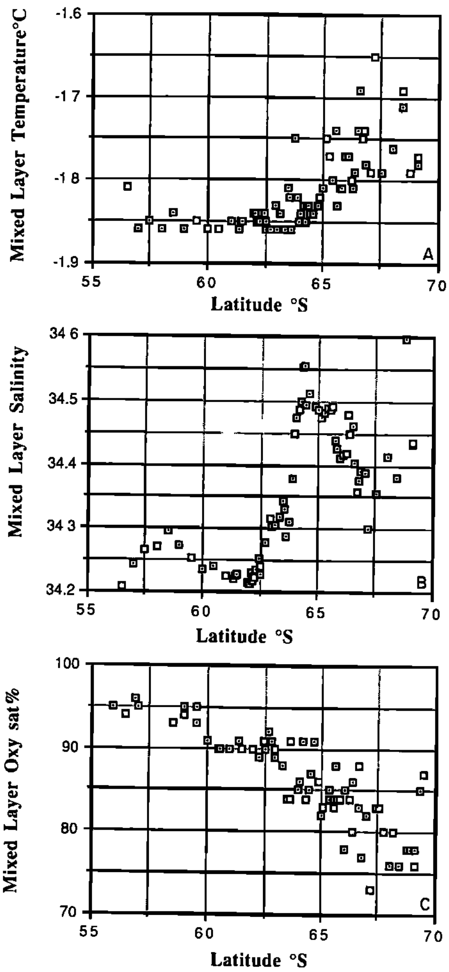

Fig. 8. Mixed layer (*a*) potential temperature, (*b*) salinity, and (*c*) oxygen saturation relative to an atmospheric pressure of 986 mbar versus latitude for stations 74–145.

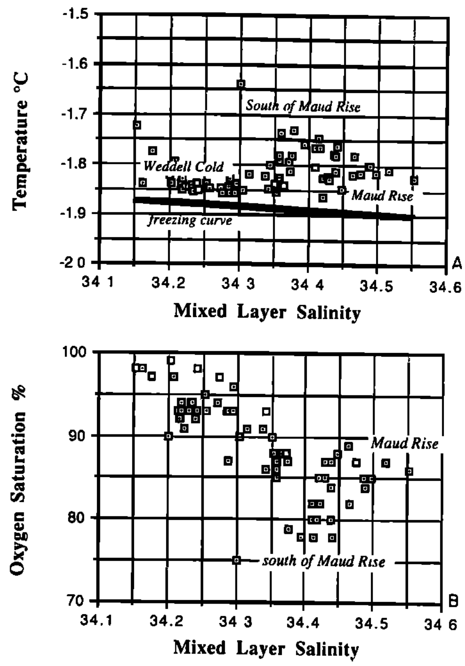

Fig. 9. (*a*) Mixed layer potential temperature versus salinity and (*b*) mixed layer salinity versus oxygen saturation.

calculation gives no details regarding the variability of entrainment during the winter, only of the integrated amount. The total deepwater heat transferred into the mixed layer increases with latitude. This does not necessarily mean that the entrainment rate is more intense further south but rather that it may have proceeded for a longer period at the time of sampling.

3.2. *WDW to Winter Mixed Layer Heat Flux, Q_f*

The winter entrainment period heat flux, Q_f (watts per square meter), may be calculated by dividing Q_t, the total heat transferred into the mixed layer by deepwater entrainment, by the duration of active entrainment. This is taken as the time since first ice cover. The undersaturation of the mixed layer at that time is believed to be a product of cooling of the summer water and entrainment of the *t*-min layer. Stations where the ice cover period was less than 20 days are removed from the calculations, since the method used to determine first ice is accurate only to within 1 week or 2. With the exception of one station at 59.5°S, only the data points south of 60°S are included in the following discussion.

The Q_f value (Figure 12) averages 41 W m^{-2}. Removing the stations situated over the crest of Maud Rise, which may be influenced by site specific processes, reduces the average to 37 W m^{-2}. The latitudinal dependence of Q_t is reduced, as the southern positions have a longer entrainment duration. The assumption made by *Gordon et al.* [1984] that the surface layer is at 100% saturation in oxygen at the time of first ice is incorrect. Using 96% oxygen saturation at first ice would lower the *Somov* winter period heat flux estimates by about 22% and leads to good agreement with the corresponding Ant V/2 results (about 25 W m^{-2}) in the 60°–62.5°S region.

3.3. *Annual WDW to Mixed Layer Heat Flux, Q_a*

In order to calculate the annual heat flux, Q_a, from deep water to the ocean surface layer, the summer period WDW to surface heat flux and the full duration of the winter entrainment period must be known.

The summer period flux is represented in the initial condition of 96% mixed layer oxygen saturation, since part of the undersaturation is derived from the incorporation of the previous winter's mixed layer into the developing fall mixed layer. An independent estimate of the WDW "contamination" of the *t*-min stratum can be made. The winter remnant *t*-min warms during the course of the summer period. While much of this warming can be derived from fluxes across the seasonal pycnocline which caps the *t*-min, some flux from below the main pycnocline is likely. It is noted above that the density change across the main pycnocline to the *t*-min is weak, less than that across the summer pycnocline layer, making it susceptible to vertical mixing processes. The summer *t*-min for the Weddell warm regime region along the Greenwich meridian as measured during the Ajax expedition is about 0.3°–0.4°C above the freezing point. For the Weddell cold regime the *t*-min is only 0.1°–0.2°C above freezing. Assuming half of the *t*-min warming is derived from diffusive flux across the underlying pycnocline beginning in the previous spring, a diffusive heat flux of 2 W m^{-2}, is calculated. This implies a K_z value of 0.2 cm^2 s^{-1}.

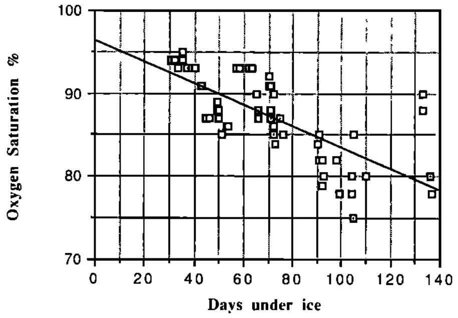

Fig. 10. Mixed layer oxygen saturation plotted against the number of days the site was cover by sea ice as determined by the Navy-NOAA ice charts and the day of the CTD observation. Because of the 1- to 2-week resolution of the Navy-NOAA ice charts, stations at sites covered by sea ice for less than 20 days are removed.

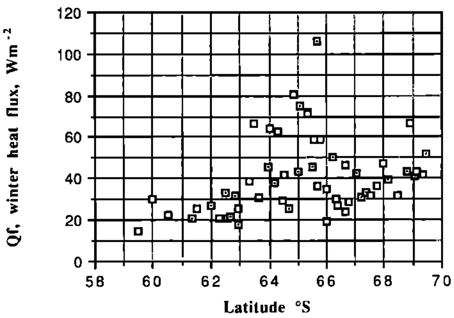

Fig. 12. Winter (period when mixed layer is covered by sea ice) heat flux, Q_f (watts per square meter), as a function of latitude (degrees south): $Q_f = Q_t$/(time under ice). Q_t is taken from Figure 11. In order to remove a large error due to first ice cover day uncertainty, only those stations at sites which were below the sea ice cover for 20 days or more are used in this figure.

Therefore approximately 2 W m^{-2} may represent the non-entrainment summer period WDW to surface layer heat flux. In the following calculations for annual heat flux the summer fluxes are taken as 2 W m^{-2}. If the summer heat flux were taken as zero, the annual heat flux would be reduced by 13%.

A reasonable estimate of the duration of the winter entrainment period can be made. We can choose among the following sets of entrainment period scenarios:

1. For the rather unrealistic situation that entrainment has ceased by the time of the observations, that all of the yearly entrainment was accomplished by the time of the observations, i.e., by midwinter, and that there is no further flux of deepwater heat into the mixed layer for the rest of the year, the annual heat flux Q_a is 8 W m^{-2}.

2. The more realistic situation that entrainment continues further into the winter (September 1 for north of 65°S and November 1 south of 65°S) yields an annual heat flux, Q_a = 16 W m^{-2} (Figure 13). Removing the Maud Rise stations reduces the annual heat flux to 14 W m^{-2}.

The rationale for the September 1 and November 1 combination is as follows:

3.3.1. *September 1 north of 65°S.* A time series of mixed layer oxygen concentration can be constructed for the region near 60°S and the Greenwich meridian (Figure 14). Comparison of the July Ant V/2 data with the end of August data near 60°S reveals a slight reduction in concentration and hence continued entrainment during the intervening period. The *Polarstern* cruise Ant V/3 obtained a few CTD stations near 60°S and the Greenwich meridian in early December 1986. Additionally, the *Somov* obtained data in early November 1981 in the same region. These data show a mixed layer oxygen concentration of 7.3–7.4 mL/L, similar to that of the *Polarstern* Ant V/3 December data. The corresponding saturation values are lower than those of the late August Ant V/2 data for the 60°S region, about 0.3 mL/L lower in concentration, implying continued entrainment. However, the *Somov* data do not follow the relationship between oxygen saturation and days under ice (Figure 10), suggesting that entrainment ceased before early November. Placement of the *Somov* data in Figure 10 indicates entrainment ceased about 75 days after first ice, which near 60°S is mid-June. Hence entrainment may have ended near 60°S toward the end of August. For lack of more definitive information, September 1 is taken as the entrainment cessation date for the region north of 65°S.

3.3.2. *November 1 south of 65°S.* The air temperatures are sufficiently cold to allow for some freezing, at least in the southern part of the region into the end of October. This is observed from the instrumented drifters set out from Ant V/2. Ten ice-locked drifters were placed out during Ant V/2

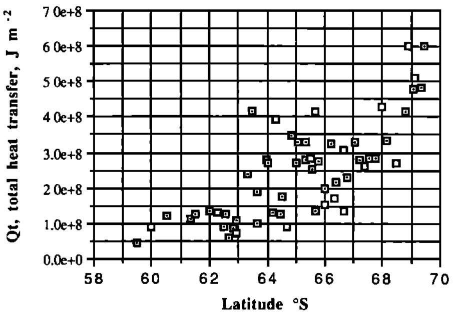

Fig. 11. Q_t (joules per square meter) introduced into the mixed layer by deepwater entrainment plotted against latitude. All stations with sufficient sampling in the mixed layer are used. This determination is based on the undersaturation of mixed layer oxygen in the 25- to 60-m interval (removed from the slightly greater variability at the top and bottom of the mixed layer), following the assumptions mentioned in the text. The mean deepwater oxygen, the local temperature of the t-max, and the thickness of the mixed layer are used for these determinations.

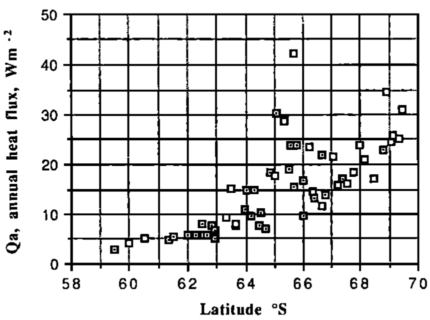

Fig. 13. Annual heat flux, Q_a (watts per square meter), as a function of latitude, assuming an entrainment period from first ice formation to September 1 north of 65°S and November 1 south of 65°S. The winter heat flux is taken from Figure 12, and the summer heat flux is taken as 2 W m^{-2} (see text). Only those stations at sites which were below the sea ice cover for 20 days or more are used in this figure.

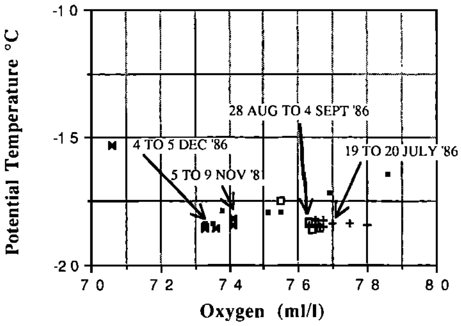

Fig. 14. Mixed layer oxygen versus potential temperature for series of stations near 60°S and the Greenwich meridian. *Polarstern* Ant V/2 data are used for the clusters of July to September 1986; *Polarstern* Ant V/3 data are used for December 1986; and *Somov* data are used for the November 1981 period.

[*Hoeber and Gube-Lehnhardt*, 1987] within the range of 60°–67.5°S. These drifters were equipped with air temperature sensors, all of which recorded significant warming to the range 0° to −5°C after October 25, 1986. For the previous month the air temperatures were closer to −10°C, with significantly more variance. As discussed below, air temperatures colder than −10°C are required to prevent ice melting. In 1986 south of 65°S it is likely that entrainment ended shortly before November 1. Additionally, *Allison* [1981], using ice growth data near Mawson Base south of Australia, finds that oceanic heat loss has a late winter maximum. While the Allison measurements were made near 62°S, they were along the coastline of Antarctica, exposed to very cold outflow of continental air masses, and hence may be indicative of heat flux variability for the southern extreme of the seasonal sea ice cover. *Lemke* [1987] also finds late winter heat flux in a one-dimensional mixed layer model for the southern ocean and attributes it to increased upward diffusion as the pycnocline is made sharper by the winter period entrainment.

4. WDW Flux Into the Mixed Layer and Compensating Freshwater Flux

The entrainment process would continuously deepen the mixed layer were it not for some restoring process, presumably the annual Ekman upwelling and perhaps, in the case of the continental margin, the translation of a sloping pycnocline. As the mixed layer deepens, the entrainment rate diminishes, and eventually, equilibrium is established. Thus for a given convective and turbulent situation within the mixed layer, stronger Ekman upwelling would result in a thinner mixed layer. The balance is achieved regionally and on an annual basis; local mesoscale features in the ocean or synoptic weather events would upset the local balance.

As deep water is incorporated into the mixed layer, mixed layer water must be removed to maintain an annual steady state situation. For the September 1/November 1 entrainment termination condition the average WDW entrainment is 45 m (Figure 15). This yields a residence time for water within the 111-m mixed layer of 2.5 years. The annual total entrainment increases to the south, attaining 100 m over Maud Rise and over the continental slope, suggesting a much reduced residence time.

The annual freshwater flux (excess of precipitation plus glacial ice melt over evaporation, $P + R - E$) must compensate the salt input of the WDW and return the surface layer salinity to the initial value. In order to calculate the freshwater input required for steady state the duration of entrainment is needed, as in the case for the heat flux calculations. With the 34.11 initial mixed layer salinity (average surface and *t*-min layer salinity obtained from the Ajax data along the Greenwich meridian from 60° to 70°S [*SIO*, 1985]) the required annual $P + R - E$ along the Greenwich meridian is 75 cm. The latitude dependence mirrors the WDW entrainment plot (Figure 15).

Estimates of the net freshwater input to the southern ocean are subject to large uncertainty, though a value of 40 cm yr^{-1} can be obtained from the literature [*Gordon*, 1981]. It appears the freshwater flux derived in this study is too large. Why? An important element in the surface layer salinity balance has not been taken into account: the loss of salty surface water during formation of AABW. For example, if half of the entrained WDW were ultimately to contribute to AABW (see section 7), with a salinity not much below the salinity of the WDW, then the required freshwater input is reduced by half to approximately 40 cm yr^{-1}. Therefore the required annual freshwater balance may not be unreasonable when the full dispersion of the surface layer is taken into account.

5. Entrainment Consequences to Sea Ice Cover

5.1. *Equilibrium Air Temperature*

Transfer of deepwater heat into the winter mixed layer is expected to have an effect on the thermodynamics of the sea ice cover. Deepwater heat introduced into the mixed layer which is not lost to the atmosphere would be available to melt ice. Conversely, if the atmosphere removes more heat than introduced from below by the deep water, freezing would ensue. To a first approximation, heat transfer from the ocean into the atmosphere depends on ice concentration (percent leads) and ice thickness, as well as on the air temperature and wind speed. The sea ice thickness observed during Ant V/2 averaged near 50 cm, with a lead occurrence of 5% [*Wadhams et al.*, 1987].

The heat available for melting sea ice is given by the difference between the entrainment heat flux and the loss to the atmosphere by conduction through the sea ice cover and by loss within leads:

$$M_i L_t = Q_f - [Q_{\text{conducton}} + Q_{\text{leads}}] \qquad (1)$$

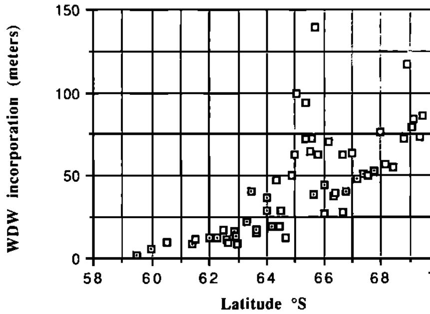

Fig. 15. Thickness (meters) of WDW incorporated into the winter mixed layer as function of latitude. Only those stations at sites which were below the sea ice cover for 20 days or more are used in this figure.

where M_i is the melting rate of the sea ice cover and L_t is the latent heat of fusion. Assuming that ocean to atmosphere heat flux is n times greater for leads than for conduction through the ice and that the ratio of leads to ice cover is given by p, (1) becomes

$$M_iL_t = Q_f - [p(n - 1) + 1]Q_{\text{conduction}} \quad (2)$$

Using the *Wadhams et al.* [1987] observations, a simple form for $Q_{\text{conduction}}$ (the sea ice value for diffusivity and a linear thermal gradient between the seawater freezing point and the air temperature) and the Q_f determined earlier (Figure 12), the air temperature which yields no net production or melting of sea ice can be determined (Figure 16). The average air temperature required to maintain the observed mean sea ice cover is −13°C. The measured average air temperature during the CTD stations was −13°C (the exact comparison is fortuitous). Therefore at the time of the Ant V/2 expedition the air temperature was, on average, just sufficient to remove from the mixed layer the heat introduced by WDW entrainment. The oscillations of air temperature due to synoptic weather would induce alternating freezing and melting episodes. In addition, there would be spatial variability, as ice would form in the leads but would melt where the ice thickness exceeds (through the action of rafting, which for a nondivergent ice field would balance ice generation in the leads) the critical value.

5.2. *Sea Ice Production*

Net sea ice production during the winter up to the time of observation can be calculated with a simple salinity budget for the mixed layer, using oxygen as a proxy indicator of WDW entrainment as is done for the thermal budgets. Entrainment of deep water introduces salt into the winter mixed layer. The salinity of the mixed layer would be determined by the ratio of deep to surface water were it not for net ice formation, precipitation, and evaporation. During the winter the latter two are not important, since the ocean surface is protected from a direct water exchange with the atmosphere by the ice cover. Positive deviations from simple mixing of surface and deep water are thus due to ice formation. The results are sensitive to the initial salinity of the surface water, which is difficult to ascertain. The average salinity of the summer surface water and t-min along the Greenwich meridian measured by the Ajax expedition is 34.11. Using this value for the initial salinity of the mixed layer in fall, with an oxygen saturation of 96% and WDW water salinity of 34.68, the mean ice formation across the full latitudinal range of Ant V/2 is 55 cm (Figure 17). The sea ice thickness distribution observed during Ant V/2 displays a mode from 40 to 60 cm [*Wadhams et al.*, 1987].

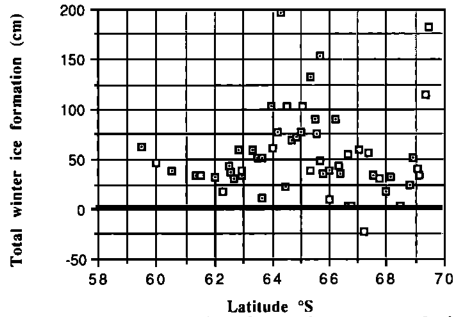

Fig. 17. Total winter sea ice formation versus latitude. The calculation yields the ice formation up to the time of the CTD station observation; however, since an equilibrium is achieved between the WDW heat flux and the ice cover, it represents the total ice formation.

The latitudinal form of the ice thickness distribution (Figure 17) is similar to that observed by *Wadhams et al.* [1987, Figure 9], but with the important exception of Maud Rise. Here the entrainment model calculates more ice than is observed. The Maud Rise values in all parameters (Q_f, WDW upwelling, ice formation) determined from the entrainment concept are all above the regional trend. It is probable that some other processes are active or that the initial conditions (at onset of sea ice) differ in the Maud Rise region. For example, the salinity of the mixed layer over Maud Rise is above the regional value of 34.11. The Ajax station 89 near Maud Rise shows a mean salinity of the surface and t-min layers of 34.21. Using a 34.2 mixed layer at the beginning of the entrainment period reduces the computed ice thickness to 70 cm. Other factors may be that the sea ice is thinner or has more leads during part of the winter (lower ice concentration is observed in the Maud Rise region by the satellite microwave data [*Comiso and Gordon*, 1987]), allowing more heat to be lost directly to the atmosphere.

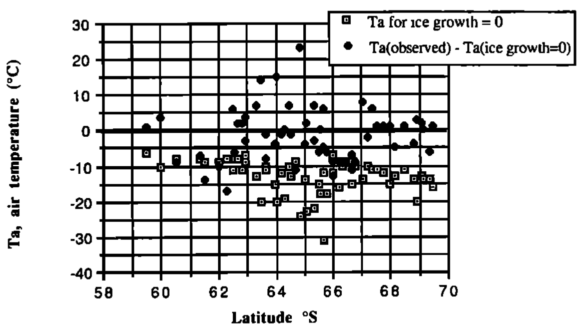

Fig. 16. Air temperature required for no net sea ice production using the entrainment heat flux from initiation of entrainment to the time of the observation (given in Figure 12). Only those stations at sites which were below the sea ice cover for 20 days or more are used in this figure.

6. The Maud Rise Anomaly

The mixed layer over Maud Rise is anomalous in a number of ways. It is not the intent of this paper to discuss fully the oceanographic processes at Maud Rise, but a number of aspects should be mentioned, as they impact on the mixed layer characteristics.

6.1. *Salty/Dense Mixed Layer*

Over Maud Rise the mixed layer salinity and density attain the highest values encountered during the expedition. The salinity is particularly high compared to the regional relationship of mixed layer oxygen to salinity. This implies high ice production over Maud Rise, though increased vertical flux of WDW may be the primary contributor, as discussed below.

The mixed layer σ_0 is 27.78, only 0.03–0.04 larger than that of the temperature maximum near 300 m (Figures 3 and 7*b*). The denser surface water over Maud Rise induces a cyclonic baroclinic circulation around the Rise, amounting to 4 cm s^{-1} for the surface geostrophic current relative to 1000 dbar (Figure 1). The buoyancy frequency across 10-dbar intervals for the stations 100–111 is 2.07 cycles h^{-1}, versus 4.67 cycles

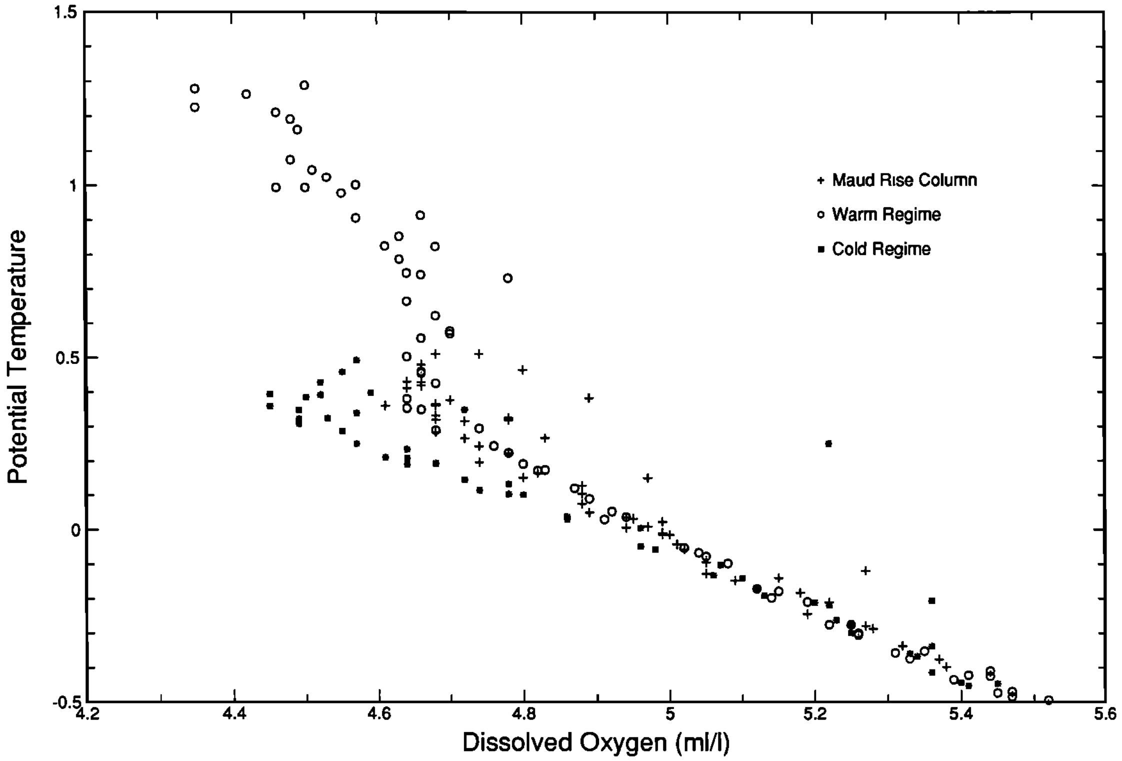

Fig. 18. Maud Rise temperature/oxygen compared to a warm and a cold regime temperature/oxygen plot.

h^{-1} for stations 116–127 to the north of Maud Rise, and 3.78 cycles h^{-1} for stations 80–90 to the south. At station 108 the salinity and σ_0 within the 20- to 100-m interval of the mixed layer attain the maximum values observed during Ant V/2: 34.516 and 27.789, respectively. At 240 m, at the temperature maximum, $\sigma_0 = 27.820$. The vertical gradient of potential density between mid mixed layer and t-max approaches zero for a reference pressure of 500 dbar ($\sigma_{0.5}$).

6.2. *Maud Rise WDW*

The t-max over Maud rise is significantly cooler than it is over the sides of the rise (Figure 4) [*Bagriantsev et al.*, 1989]. The t-max over the crest is about the same as that measured further north within the cold regime of the Weddell Gyre. However, the oxygen concentration at the Maud Rise t-max does not display the telltale minimum of the cold regime (Figures 6*b* and 18); it is 0.2 mL/L higher than it is within the Weddell cold regime. Comparison of the Maud Rise water column with that of the surrounding ocean (Figure 19) indicates that the Maud Rise column can be achieved by a 400-m upward displacement of the surrounding water column. Not knowing the residence time of the water within the Maud Rise water column or the area of the source region relative to that of the Maud Rise crest prohibits determination of the mean vertical velocity. A residence time of 1 year implies a vertical velocity of 1.3×10^{-5} m s^{-1} for a 1 : 1 ratio of source to crest area.

6.3. *Isopycnal Mixing*

The relatively dense mixed layer over Maud Rise forces density surfaces which are ordinarily embedded within the regional temperature maximum of the WDW to pass into the mixed layer and have direct isopycnal access to the winter atmosphere. The t-max density within the warm WDW over the sides of the rise is near $\sigma_0 = 27.76$–27.78, the same as the Maud Rise mixed layer. Gradients of temperature on the 27.78 isopycnal range from the t-max of 1.1°C to −1.8°C in the mixed layer in a distance of about 200 km (with a maximum change of 0.9°C in only 50 km). Using a lateral mixing coefficient of 10^2 m^2 s^{-1} (characteristic for a 100-km horizontal scale [*Okubo*, 1971]) and a 100-km radius for the Maud Rise anomaly, a 100-m slab of ocean centered at $\sigma_0 = 27.78$ would represent a flux of slightly more than 10 W m^{-2} into the Maud Rise mixed layer. This flux would be accompanied by the same WDW salinity and oxygen that would be associated with the entrainment process. Therefore 20% of the heat flux into the Maud Rise mixed layer, attributed to entrainment, may be due to isopycnal mixing. Signs of isopycnal mixing can be seen in the θ/S structure of the WDW temperature maximum (Figure 20). The thermohaline fine structure, aligned along isopycnals, portrays a situation in which the warmer WDW is transferring heat and salt directly into the mixed layer. Clearly, the number used for the mixing coefficient and the 100-m slab over which the isopycnal process is active are merely reasonable guesses, but it is suggested that for the Maud Rise region a one-dimensional treatment may be insufficient.

6.4. *Circulation-Topography Interaction*

The unique water column characteristics of Maud Rise must be related to the interaction of the rise with the larger-scale circulation. *Roden* [1987] and *Bagriantsev et al.* [1989] briefly review the various attempts to model flow over isolated topographic highs or seamounts [*McCartney*, 1976; *Boyer et al.*, 1984; *Huppert and Bryan*, 1976] which show patterns similar to that observed in 1984: isolated Taylor Columns (closed circu-

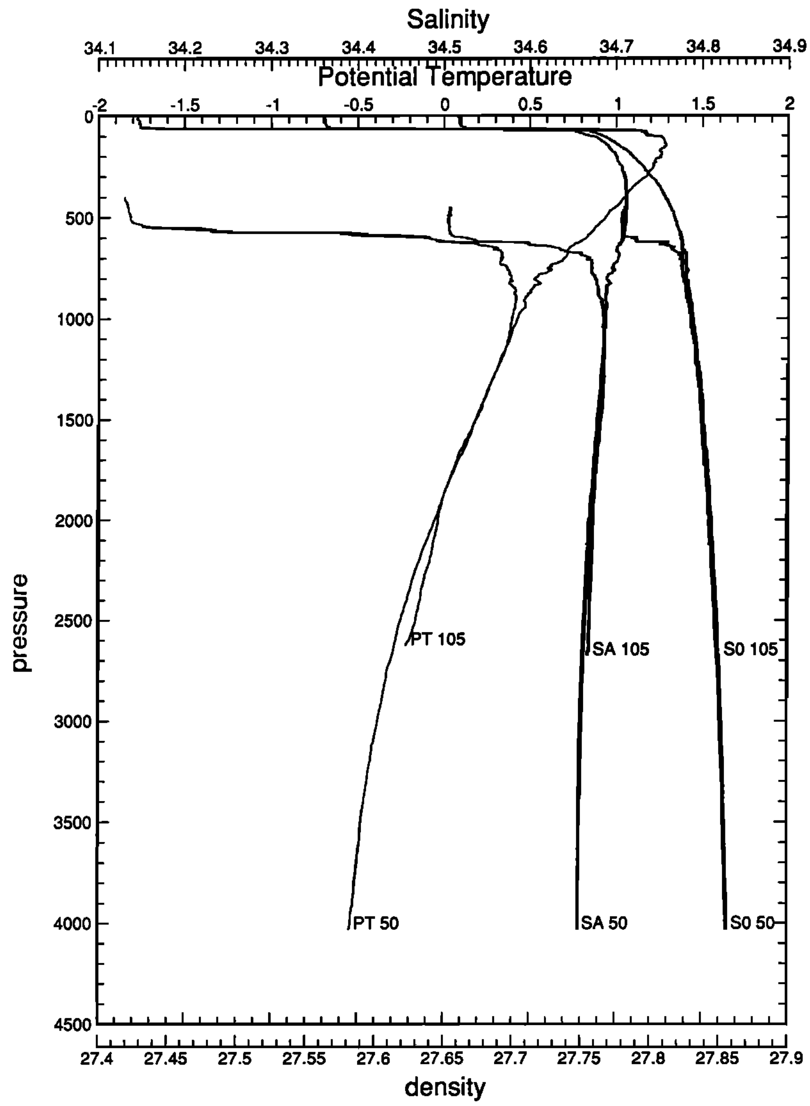

Fig. 19. Comparison of the thermohaline stratification over the crest of Maud Rise with that over the flanks of the rise. In order to match the profiles the water column over the flanks needs to be upwelled by 400 m.

lation cells) developed over the topographic high with various waves and eddies forming downstream of the topographic feature. None of the models are specifically applicable to the high-amplitude Maud Rise situation, but they do provide a sense of what to expect. *Huppert and Bryan* [1976] develop an *f*-plane model for a linear stratified water column passing over a low-amplitude isolated topographic high. A denser (colder) water column forms over the topographic high. A less dense (warmer) water column develops downstream, where it remains for low-flow conditions and advects downstream for high-flow conditions. As stratification increases, the flow passes around the topographic high, rather than flowing over it.

7. DISCUSSION

7.1. *Circumpolar Extrapolation*

7.1.1. *Heat flux.* *Gordon* [1981] estimated the ocean to atmosphere annual heat flux for the circumpolar belt 60°–70°S, using climatological data with bulk aerodynamic equations, as 31 W m^{-2}. The annual heat flux value determined in this study for the 60°S to 70°S segment along the Greenwich meridian is 16 W m^{-2} (14 W m^{-2} without the Maud Rise stations). The winter period heat flux determined is 41 W m^{-2} (37 W m^{-2} without Maud Rise). The heat flux across 60°S given by *Gordon* [1981] is 5.4 × 10^{14} W s^{-1}. The value determined here is about half: 2.8 × 10^{14} W s^{-1}. Inclusion of Maud Rise in circumpolar extrapolation is meant to incorporate various unique situations of circulation/topographic enhancement of WDW upwelling. While the present numbers are less than the values determined in the 1981 study, it must be pointed out that (1) the 1981 calculations use meteorological data for the winter period which are primarily determined by interpolation, not direct observations, and must be considered as rough approximations; and (2) the calculations performed in this study would underestimate the total heat flux across 60°S, since only the open ocean situation of mixed layer stratification is represented, and the continental margin effects associated with AABW formation are not included. The 2.8 × 10^{14} W s^{-1} value should be taken as a lower bound for heat flux across 60°S, as it includes only part of the total heat loss to the atmosphere south of 60°S.

7.1.2. *WDW flux.* The winter mixed layer oxygen un-

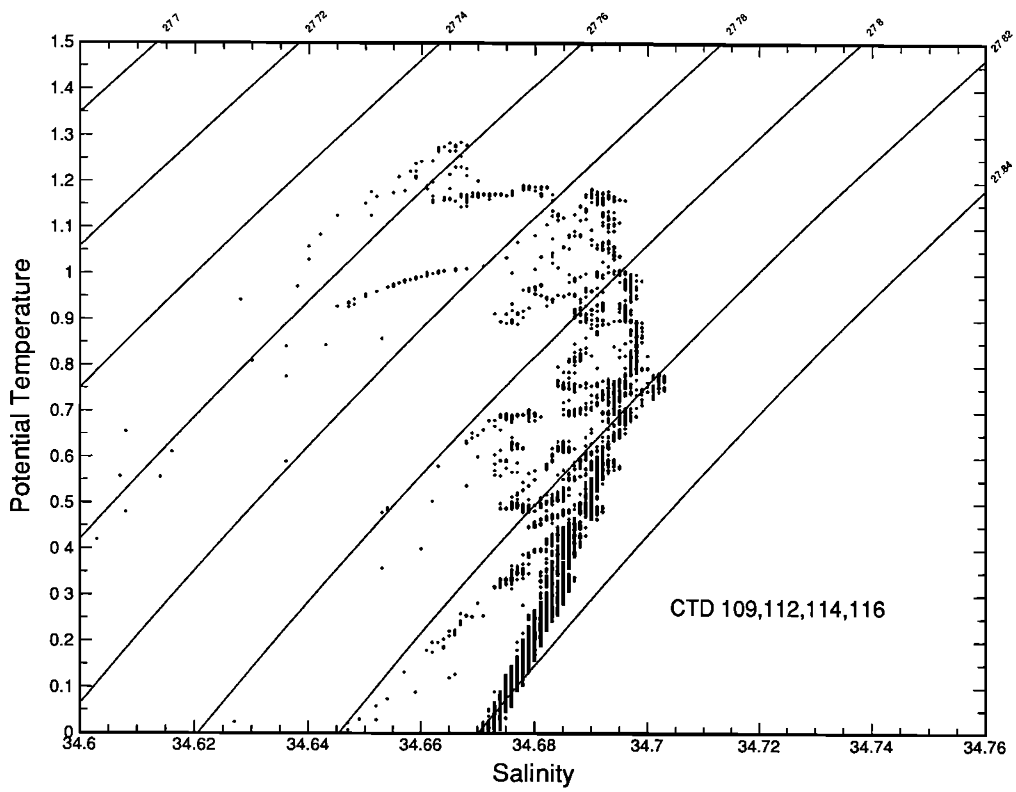

Fig. 20. Group θ/S of a sequence of CTD stations along the flanks of Maud Rise.

dersaturation implies an average upwelling of WDW of 45 m yr^{-1}. Applying this value to the full circumpolar region in the 60°S to 70°S band yields 24×10^6 m^3 s^{-1}. *Levitus* [1988] estimates the northward Ekman volume flux across 60°S as 10×10^6 m^3 s^{-1}. An additional loss of deep water entering the surface layer is that contributing to the formation of AABW. Thus about 42% of the entrained WDW is withdrawn from the surface layer within the Ekman layer across 60°S, and the remaining 14×10^6 m^3 s^{-1} is available to sink with AABW. The total production of AABW involves more than the surface end-member, in that deep water is incorporated into the blend within the shelf processes or by entrainment into the sinking slope plumes. If the surface water component (open ocean and shelf water) comprises about 80% of the total AABW formation, as suggested in the recipe of *Foster and Carmack* [1976], a AABW production rate of 17.5×10^6 m^3 s^{-1} is implied. A 50 : 50 mix of surface to other water masses, which represents the more traditional recipe, results in 28×10^6 m^3 s^{-1} AABW production. *Jacobs et al.* [1985] estimated the AABW formation rate along the continental margin as 13×10^6 m^3 s^{-1}. *Gordon* [1975], using a large-scale thermal balance, estimated the total AABW production as 38×10^6 m^3 s^{-1}. This is in agreement with a AABW production rate of 41×10^6 m^3 s^{-1} determined from ^{14}C considerations of *Stuiver et al.* [1983]. In view of the uncertainties the WDW flux obtained from the mixed layer calculations of this study results in AABW production at a rate within the expected range.

7.2. *Maud Rise and Polynyas*

This study along with the modeling study of *Martinson* [this issue] indicates that the extensive winter sea ice cover of the southern ocean is limited in its thickness by mixed layer entrainment of the relatively warm and salty deep water. One can conceive of a network of negative feedbacks that produces a relatively stable but thin veneer of sea ice. The sea ice cover and ocean static stability are maintained by salinity; this is referred to as the salinity mode. However, the stable salinity mode configuration can be upset. The Weddell Polynya of the mid-1970s [*Carsey*, 1980; *Martinson et al.*, 1981; *Gordon*, 1982] is a dramatic example that another stable mode can exist.

In the polynya condition the ocean stratification is destroyed, and vigorous convection persists, eliminating the sea ice cover. This configuration is driven by heat and is referred to as the thermal mode. The conversion of the more common salinity mode to the anomalous thermal mode requires the salinity of the winter mixed layer to become sufficiently high to force free convection within the ocean. The convection continues as the upwelled water is cooled by contact with the atmosphere. This thermal mode can be shut down only if enough fresh water is added to the surface layer [*Martinson et al.*, 1981]. Transient polynyas, frequently observed over the deep ocean [*Comiso and Gordon*, 1987], are examples of a thermal mode being shut down by an influx of sea ice from the surrounding ocean.

The appearance of the Weddell Polynya in the mid-1970s and smaller more transitory polynyas in the Maud Rise region suggests a relationship of horizontal and vertical circulation in the vicinity of Maud Rise to the winter sea ice cover. The less than 100-km horizontal scale and the more-or-less fixed location of the recurrent polynya suggest an oceanic origin, rather than an effect of the localized wind field. It is suggested that the enhanced upwelling over Maud

Rise area is due to interaction between circulation and bottom topography, sensitizing that region to polynya development by introducing more salty WDW into the mixed layer than is provided by the regional Ekman upwelling process. The Maud Rise effect is an external factor which boosts the mixed layer salinity and density to the critical value, allowing convection.

Martinson et al. [1981] show that a shallow pycnocline is an effective preconditioner for deep-reaching convection associated with polynya generation. The regional depth of the pycnocline is set by a balance of the winter entrainment process with the annual wind-induced upwelling. Spin-up of the regional wind field would increase the baroclinic vigor of the Weddell Gyre. The associated upwelling may then draw more warm/saline CDW into the gyre and, if all else stays constant, would result in a thinner saltier mixed layer and more susceptibility to polynyas. However, the enhanced upwelling over Maud Rise, relative to the regional Ekman-induced upwelling, may allow for a faster barotropic response.

Studies of the interaction between topography and circulation indicate that upwelling over Maud Rise would increase as the larger-scale horizontal flow increases (H. W. Ou, personal communication, 1989). The immediate effect of an increase of the regional wind stress curl will be to spin up the barotropic circulation component. Increased upwelling over Maud Rise would transfer additional salt into the mixed layer and make the area more susceptible to polynya generation.

The sequence of events leading to a polynya may be as follows: (1) An increase of the regional wind field curl spins up the barotropic circulation of the Weddell Gyre. (2) Upwelling over topographic features, such as Maud Rise, increases. (3) The vulnerability for a switch-over from the salinity (sea-ice-covered) mode to the thermal convective (polynya) mode is enhanced as more salt is delivered to the overlying mixed layer.

If the spatial scale of the topography-induced upwelling is extensive, the convective region may be large enough to form a self-protective barrier to freshwater influx from the sides. This occurred in the Weddell Gyre in the mid-1970s over Maud Rise. Eventually, shutdown occurred as the general circulation advected the convective region into the western Weddell Sea where strong sea ice convergence was able overwhelm the thermal mode.

8. Conclusions

Table 1 summarizes the flux determinations based on the Ant V/2 mixed layer data and provides estimates of probable uncertainties. These results are important for a number of reasons: (1) They are of direct relevance to the vertical exchange of heat, fresh water, gases, and nutrients between the deep ocean and the atmosphere, as well as to the thermodynamics of the ice cover. (2) The extent of the Maud Rise anomaly and associated circulation-topographic-induced upwelling is better defined. (3) The results can be used to guide, test, and further refine mixed layer models [e.g., *Martinson*, this issue]. (4) The results can be used for the design of more specific field experiments to obtain more quantitative information on the subtle interplay between sea ice, mixed layer, and atmospheric processes. For example, it is clear that the calculations reported here are very sensitive to initial conditions of the mixed layer immediately prior to sea ice formation and that autumn season measurements are needed to help constrain the calculations and models. (5) The results suggest a sequence of events that may spur polynya development.

TABLE 1. Average Values for Vertical Fluxes for the Region 59.5°–69.5°S Along the Greenwich Meridian

	Value
Winter heat flux from the WDW* to the mixed layer, Q_f	41 ± 4 W m^{-2}†
Annual heat flux from the WDW* to the mixed layer, Q_a	16 ± 2 W m^{-2}‡
WDW incorporated into the winter mixed layer	45 ± 9 m yr^{-1}§
Sea ice production to the time of the observations	55 ± 15 cm‖
Equilibrium air temperature, t_a	$-13° \pm 2$°C¶
Circumpolar extrapolation	
Heat flux across 60°S, $Q_{60°}$	$2.8 \pm 0.35 \times 10^{14}$ W
Total WDW upwelling	$24 \pm 5 \times 10^6$ m^3 s^{-1}

*WDW is Weddell Deep Water.

†Q_f is sensitive to the initial oxygen saturation of the mixed layer immediately prior to ice formation. As described in the text, the saturation value used for this calculation is derived from data to be approximately 96%. Q_f changes by 5% as the initial oxygen saturation is changed by 1 percentage point. A probable uncertainty of ±4 W m^{-2} is assigned to Q_f, corresponding to a reasonable uncertainty of 4 percentage points for initial oxygen saturation. Oxygen flux from the atmosphere into the ocean during the winter is considered to be insignificant.

‡Annual heat flux would have an error similar to that of Q_f because of uncertainty in the initial oxygen saturation value. Additional uncertainty is due to the estimation of the summer heat flux (which is estimated from seasonal warming of the remnant winter *t*-min layer), though this factor is a minor contributor to Q_a. A ±2 W m^{-2} error is estimated for Q_a.

§As with the winter heat flux value, WDW upwelling into the winter mixed layer is sensitive to the initial oxygen saturation of the mixed layer immediately prior to ice formation. A 1 percentage point change in initial oxygen saturations yields a 10% change in WDW upwelling. An uncertainty of ±9 m yr^{-1} is estimated for WDW upwelling which corresponds to a 4 percentage point spread of initial oxygen saturation.

‖Since an equilibrium of WDW heat flux and ice thickness is achieved by midwinter, this value effectively represents the total winter ice formation. The sea ice formation is very sensitive to the initial salinity of the mixed layer. This is determined to be 34.11 from summer data. Sea ice formation changes by 57% for every 0.1 change in salinity. Since this is the probable uncertainty in initial salinity, the uncertainty of sea ice formation is estimated as ±30 cm, corresponding to a spread of initial salinity of 0.2.

¶The equilibrium air temperature, t_a, is that required to balance the winter WDW to mixed layer heat flux by removing the heat to the atmosphere, by preventing net freezing, or by melting of sea ice. The value is derived from observed parameters. As the lead area changes by 1 percentage point, t_a changes by only 1°C. Changes in sea ice thickness of 20% or flux enhancement over leads relative to the ice-covered situation of 50% alter t_a by 2°C. The estimated uncertainty in t_a is taken as ±2°C.

Acknowledgments. The data collection and analysis was supported by the Division of Polar Programs of the National Science Foundation, grant DPP 8502386. We thank the Alfred Wegener Polar Institute in Bremerhaven, FRG, and its Director, G. Hempel, for the opportunity to participate in the Winter Weddell Sea Expedition of 1986 of the *Polarstern*. We thank E. Augstein, Chief Scientist on *Polarstern* cruise Ant V/2, for orchestrating a fine and effective cruise among a diverse set of characters and unexpected circumstances. Discussions with Doug Martinson have been helpful in developing many of the ideas presented in this study. Lamont-Doherty Geological Observatory contribution 4633.

REFERENCES

Allison, I., Antarctic sea ice growth and oceanic heat flux, *IAHS Publ.*, *131*, 161–170, 1981.

Bagriantsev, N. V., A. L. Gordon, and B. A. Huber, Weddell Gyre: Temperature maximum stratum, *J. Geophys. Res.*, *94*, 8331–8334, 1989.

Boyer, D., P. Davies, and W. Holland, Rotating flow past disks and cylindrical depressions, *J. Fluid Mech.*, *141*, 67–95, 1984.

Carsey, F. D., Microwave observations of the Weddell Polynya, *Mon. Weather Rev.*, *108*, 2032–2044, 1980.

Clarke, A. R., J. H. Swift, J. L. Reid, and K. P. Koltermann, The formation of Greenland Sea Deep Water: Double diffusion or deep convection?, *Deep Sea Res.*, in press, 1990.

Comiso, J., and A. L. Gordon, Recurring polynyas over the Cosmonaut Sea and the Maud Rise, *J. Geophys. Res.*, *92*, 2819–2833, 1987.

Deacon, G. E. R., The Weddell Gyre, *Deep Sea Res.*, *26*, 981–995, 1979.

Foster, T. D., and E. C. Carmack, Frontal zone mixing and Antarctic bottom water formation in the southern Weddell Sea, *Deep Sea Res.*, *23*, 301–317, 1976.

Gordon, A. L., General ocean circulation, Numerical Models of Ocean Circulation, publication, pp. 39–53, Natl. Acad. of Sci., Washington, D. C., 1975.

Gordon, A. L., Seasonality of southern ocean sea ice, *J. Geophys. Res.*, *86*, 4193–4197, 1981.

Gordon, A. L., Weddell Deep Water variability, *J. Mar. Res.*, *40*, suppl., 199–217, 1982.

Gordon, A. L., The southern ocean and global climate, *Oceanus*, *31*(2), 39–46, 1988.

Gordon, A. L., and B. A. Huber, Thermohaline stratification below the southern ocean sea ice, *J. Geophys. Res.*, *89*, 641–648, 1984.

Gordon, A. L., and W. D. Nowlin, The basin waters of the Bransfield Strait, *J. Phys. Oceanogr.*, *8*(2), 258–264, 1978.

Gordon, A. L., C. T. A. Chen, and W. G. Metcalf, Winter mixed layer entrainment of Weddell Deep Water, *J. Geophys. Res.*, *89*, 637–640, 1984.

Hoeber, H., and M. Gube-Lehnhardt, The eastern Weddell Sea drifting buoy set of the Winter Weddell Project (WWSP) 1986, *Ber. Polarforsch.*, *37*, 1–108, 1987.

Houssais, M.-N., Testing a coupled ice-mixed layer model under Subarctic conditions, *J. Phys. Oceanogr.*, *18*, 196–210, 1988.

Huber, B. A., P. A. Mele, W. E. Haines, A. L. Gordon, J. C. Jennings, L. I. Gordon, R. F. Weiss, F. A. Van Woy, and P. K. Salameh, CTD and hydrographic data from cruise ANT V/2 of R/V *Polarstern*, *Tech. Rep. LDGO-89-3*, Lamont-Doherty Geol. Obs., Palisades, N. Y., 1989.

Huppert, H. E., and K. Bryan, Topographically generated eddies, *Deep Sea Res.*, *23*, 655–680, 1976.

Jacobs, S., R. Fairbanks, and Y. Horibe, Origin and evolution of water masses near the Antarctic continental margin: Evidence from $^{18}O/^{16}O$ ratios in seawater, in *Oceanology of the Antarctic Continental Shelf, Antarctic Res. Ser.*, vol. 43, edited by S. S. Jacobs, pp. 59–85, AGU, Washington, D. C., 1985.

Lemke, P., A coupled one-dimensional sea ice–ocean model, *J. Geophys. Res.*, *92*, 13,164–13,172, 1987.

Levitus, S. Ekman volume fluxes for the world ocean and individual ocean basins, *J. Phys. Oceanogr.*, *18*, 271–279, 1988.

Liss, P., and L. Merlivat, Air-sea gas exchange rates: Introduction and syntheses, in *The Role of Air-Sea Exchange in Geochemical Cycling*, edited by P. Buat-Menard, D. Reidel, Hingham, Mass., 1986.

Martinson, D. G., Evolution of the southern ocean winter mixed layer and sea ice; Open ocean deepwater formation and ventilation, *J. Geophys. Res.*, this issue.

Martinson, D. G., P. D. Killworth, and A. L. Gordon, A convective model for the Weddell Polynya, *J. Phys. Oceanogr.*, *11*, 466–488, 1981.

McCartney, M., The interaction of zonal currents with topography with applications to the southern ocean, *Deep Sea Res.*, *23*, 413–428, 1976.

Okubo, A., Oceanic diffusion diagrams, *Deep Sea Res.*, *18*, 789–802, 1971.

Reid, J. L., Oxygen saturation in near-surface ocean waters (abstract), *Eos Trans. AGU*, *64*, 1062, 1983.

Roden, G., Effect of seamounts and seamount chains on ocean circulation and thermohaline structure, in *Seamounts, Islands, and Atolls*, *Geophys. Monogr. Ser.*, vol. 43, edited by B. H. Keating, et al., pp. 335–354, AGU, Washington, D. C., 1987.

Røed, L. P., A thermodynamic coupled ice-ocean model of the Marginal Ice Zone, *J. Phys. Oceanogr.*, *14*, 1921–1929, 1984.

Schlosser, P., W. Roether, and G. Rohardt, Helium-3 balance of the upper layers of the northwestern Weddell Sea, *Deep Sea Res.*, *34*, 365–377, 1987.

Schnack-Schiel, H., The winter-expedition of RV *Polarstern* to the Antarctic (Ant V/1-3), *Ber. Polarforsch.*, *39*, 1–259, 1987.

Scripps Institution of Oceanography, Physical, chemical and in-situ CTD data from the Ajax Expedition in the South Atlantic Ocean, aboard RV *Knorr*, leg I: 7 October–6 November 1983, leg II: 11 January–19 February 1984, Ajax data report, *Ref. 85-24*, Univ. of Calif., San Diego, 1985. (Available as *Ref. 85-4-D* from Dep. of Oceanogr., Tex. A&M Univ., College Station, 1985.)

Shay, T. J., and M. C. Gregg, Convectively driven turbulent mixing in the upper ocean, *J. Phys. Oceanogr.*, *16*, 1777–1798, 1986.

Stuiver, M., P. Quay, and H. Östlund, Abyssal water carbon-14 distribution and the age of the world ocean, *Science*, *219*, 849–851, 1983.

Van Loon, H., Pressure in the southern hemisphere, in *Meteorology of the Southern Hemisphere*, *Meteorol. Monogr. Ser.*, vol. 13(35), edited by C. W. Newton, pp. 59–86, American Meteorological Society, Boston, Mass., 1972.

Wadhams, P., M. A. Lange, and S. F. Ackley, The ice thickness distribution across the Atlantic sector of the Antarctic Ocean in midwinter, *J. Geophys. Res.*, *92*, 14,535–14,552, 1987.

Weiss, R., Winter Weddell Sea Project 1986: Trace gas studies during legs Ant V/2 and V/3 of *Polarstern*, *Antarct. J.*, *22*(5), 99–100, 1987.

Weiss, R. F., H. G. Ostlund, and H. Craig, Geochemical studies of the Weddell Sea, *Deep Sea Res.*, *26*, 1093–1120, 1979.

Whitworth, T., III, and W. Nowlin, Water masses and currents of the southern ocean at the Greenwich meridian, *J. Geophys. Res.*, *92*, 6462–6476, 1987.

A. L. Gordon and B. A. Huber, Lamont-Doherty Geological Observatory, Columbia University, Palisades, NY 10964.

(Received September 18, 1989;
accepted December 7, 1989.)